

## Radiation interaction with tilt grain boundaries in $\beta$ -SiC

Narasimhan Swaminathan, Marcin Wojdyr, Dane D. Morgan, and Izabela Szlufarska

Citation: *Journal of Applied Physics* **111**, 054918 (2012); doi: 10.1063/1.3693036

View online: <http://dx.doi.org/10.1063/1.3693036>

View Table of Contents: <http://scitation.aip.org/content/aip/journal/jap/111/5?ver=pdfcov>

Published by the [AIP Publishing](#)

---

### Articles you may be interested in

[Role of  \$\Sigma 5\$ , \(210\), \[001\] CSL boundary on displacement cascade in bcc Fe](#)

*AIP Conf. Proc.* **1447**, 743 (2012); 10.1063/1.4710217

[Kapitza conductance of symmetric tilt grain boundaries in graphene](#)

*J. Appl. Phys.* **111**, 053529 (2012); 10.1063/1.3692078

[Shock wave loading and spallation of copper bicrystals with asymmetric  \$\Sigma 3\$  110 tilt grain boundaries](#)

*J. Appl. Phys.* **108**, 093526 (2010); 10.1063/1.3506707

[Spatially resolved distribution of dislocations and crystallographic tilts in GaN layers grown on Si\(111\) substrates by maskless cantilever epitaxy](#)

*J. Appl. Phys.* **100**, 053103 (2006); 10.1063/1.2234807

[Large  \$T\_c\$  depression at low angle \[100\] tilt grain boundaries in bulk Bi<sub>2</sub>Sr<sub>2</sub>CaCu<sub>2</sub>O<sub>8+ \$\delta\$</sub>  bicrystals](#)

*Appl. Phys. Lett.* **70**, 1164 (1997); 10.1063/1.118514

---

Frustrated by old technology?      Is your AFM dead and can't be repaired?      Sick of bad customer support?



**It is time to upgrade your AFM**  
Minimum \$20,000 trade-in discount for purchases before August 31st

**Asylum Research is today's technology leader in AFM**

[dropmyoldAFM@oxinst.com](mailto:dropmyoldAFM@oxinst.com)

**OXFORD INSTRUMENTS**  
The Business of Science®

## Radiation interaction with tilt grain boundaries in $\beta$ -SiC

Narasimhan Swaminathan,<sup>1</sup> Marcin Wojdyr,<sup>2</sup> Dane D. Morgan,<sup>1,3,a)</sup>  
and Izabela Szlufarska<sup>1,3,b)</sup>

<sup>1</sup>Materials Science and Engineering Department, University of Wisconsin – Madison, Madison, Wisconsin 53706-1595, USA

<sup>2</sup>Institute of High Pressure Physics UNIPRESS, ul. Sokolowska 29/37, 01-142 Warsaw, Poland

<sup>3</sup>Materials Science Program, University of Wisconsin-Madison, Madison, Wisconsin 53706-1595, USA

(Received 31 October 2011; accepted 11 February 2012; published online 15 March 2012)

Interaction between grain boundaries and radiation is studied in 3C-SiC by conducting molecular dynamics cascade simulations on bicrystal samples with different misorientation angles. The damage in the in-grain regions was found to be unaffected by the grain boundary type and is comparable to damage in single crystal SiC. Radiation-induced chemical disorder in the grain boundary regions is quantified using the homonuclear to heteronuclear bond ratio ( $\chi$ ). We found that  $\chi$  increases nearly monotonically with the misorientation angle, which behavior has been attributed to the decreasing distance between the grain boundary dislocation cores with an increasing misorientation angle. The change in the chemical disorder due to irradiation was found to be independent of the type of the grain boundary. © 2012 American Institute of Physics. [<http://dx.doi.org/10.1063/1.3693036>]

### I. INTRODUCTION

Because of its outstanding mechanical properties<sup>1–6</sup> and low neutron capture cross section, silicon carbide ( $\beta$ -SiC) is considered a promising structural material for applications in advanced nuclear reactors.<sup>7,8</sup> One of the major concerns with SiC is its tendency to amorphize under radiation at low (<500 K) temperatures, which leads to undesired volume swelling<sup>9</sup> and degradation of mechanical properties.<sup>10</sup> In recent years a considerable number of studies have been dedicated to investigating the hypothesis that radiation resistance of materials can be possibly improved by decreasing the grain size to the nanometer regime. Indeed enhancement in radiation resistance due to grain size to refinement have been reported from experiments on many materials, such as Pd,<sup>11</sup> (Gd<sub>2</sub>Ti<sub>0.65</sub>Zr<sub>0.35</sub>)<sub>2</sub>O<sub>7</sub>,<sup>12</sup> MgGa<sub>2</sub>O<sub>4</sub>,<sup>13</sup> and TiN.<sup>14</sup> It has been postulated that grain boundaries (GBs) act as sinks for radiation-induced defects and therefore increasing the volume fraction of GBs leads to a faster annihilation of defects and enhanced resistance to radiation-induced amorphization.<sup>12,13</sup> However, other experiments have been reported where nanocrystalline (nc) materials showed a decreased radiation resistance as compared to their polycrystalline counterparts. Examples include studies on ZrO<sub>2</sub> (Ref. 16) and on Cu nanocrystals embedded in SiO<sub>2</sub> matrix.<sup>17</sup> One possible explanation for this observation is that an increased volume fraction of GBs increases free energy of the system (due to the interfacial energy) and as a result it may be easier to amorphize the material during radiation. Composition and microstructure are not the only parameters that control radiation resistance. For example, Chimi *et al.*<sup>15</sup> showed for Au that the nanomaterial can be worse or better than the polycrystalline counterpart depending on the

temperature. The seemingly contradicting experimental reports have inspired many computational groups to perform molecular dynamics (MD) simulations of radiation cascades in nc materials and to determine fundamental atomic-level interactions of radiation defects with GBs.<sup>18–30</sup> For example, Samaras *et al.*<sup>18–20</sup> observed that for irradiated nc Ni and nc Fe, interstitials diffusing under a stress gradient are absorbed by the GB while the vacancies remain in the grain, resulting in truncated stacking fault tetrahedra. Stoller *et al.*<sup>21</sup> noted that the number of in-grain interstitials in nc Fe increases with an increasing grain size and asymptotically approaches defect numbers in single crystal (sc) Fe. Millet *et al.*<sup>22,23</sup> investigated migration of defects in irradiated Mo and demonstrated that long annealing times of about 259 and 779 ps at temperatures as high as 2300 K (75% of the melting temperature of Mo) were needed for interstitials and vacancies, respectively, to migrate and be absorbed by a GB.

In order to better understand the specific interactions of radiation-induced defects with a GB it is useful to focus modeling on just one GB at a time, which can be conveniently done with MD simulations performed on bicrystals. Such simulations allow complete control of the distance and direction of the primary knock-on atom (PKA) with respect to the GB and yield the influence of a specific GB without the affects of other GBs that might be present in a nc system. For instance, Bai *et al.*<sup>24</sup> carried atomistic simulations on Cu bicrystal with a symmetric tilt  $\Sigma 11 \langle 110 \rangle \{131\}$  GB and discovered that such GB can act not only as a sink, but also can eject interstitials which in turn can annihilate the vacancies present in the grain interior. Brutzel *et al.*<sup>28–30</sup> conducted MD simulations of displacement cascades on UO<sub>2</sub> bicrystals and considered six different symmetric tilt GBs ( $\Sigma 41$ ,  $\Sigma 25$ ,  $\Sigma 13$ ,  $\Sigma 5$ ,  $\Sigma 29$ , and  $\Sigma 17$ ). These authors<sup>28,29</sup> found that the cascade morphology was asymmetric when the GB misorientation angle was larger than 20°, which corresponds to  $\Sigma 5$ ,  $\Sigma 29$ , and  $\Sigma 17$ . Furthermore, it was reported

<sup>a)</sup>Electronic mail: ddmorgan@wisc.edu.

<sup>b)</sup>Electronic mail: szlufarska@wisc.edu.

that there was more damage in bicrystals than in a single crystal sample, with the damaged being localized in regions near the GBs. More recently Bai *et al.*<sup>31</sup> performed a multi-time scale investigation of radiation damage near symmetric GBs in rutile TiO<sub>2</sub>. The authors studied the effect of PKA distance from the GB on the nature of defect production. They found that the GB absorbs more interstitials than vacancies when the PKA is at certain distance from the GB. The cascades produced many interstitial and vacancy clusters which were analyzed for their migration properties (pathways and barriers) using temperature accelerated dynamics.

Despite the technological importance of SiC, there have been only a few studies on radiation effects in nc SiC. Jiang *et al.*<sup>32</sup> reported that the dose to amorphize nc SiC with 4.6 nm sized grains at room temperature using Au<sup>2+</sup> ions was the same as that of the bulk material. This lack of improvement in radiation resistance of the nc material was attributed to sluggish defect transport at room temperature and to the fast ion flux that was used to conduct the experiment. Later on, the same group<sup>33</sup> conducted radiation of nc SiC with smaller grain sizes (2.0–3.8 nm), at higher temperatures (400 K), and using lighter Si<sup>+</sup> ions. It was found that for all the grain sizes under study, the dose to amorphization was lower for the nc samples than for single crystal material. The authors argued that the mechanisms of amorphization were likely different in the samples with grain size of 2.0–3.8 nm (which showed a decreased radiation resistance) than in the earlier studies on samples with grain size of 4.6 nm (which did not show a change in radiation resistance as compared to a single crystal). It was postulated that in the smaller grain samples,<sup>33</sup> the amorphization was an ion-induced interface driven process with the onset of amorphization in the unstable, amorphous GB regions. In the larger grain sizes, the amorphization was argued to more or less driven by the accumulation of point defects, similarly to what happens in the bulk material.

A few MD simulations of radiation effects in SiC samples that contain GBs have been recently reported.<sup>25–27</sup> Swaminathan *et al.*<sup>25</sup> carried out cascade simulations in nc and sc 3C-SiC and concluded that on average, GBs do not affect the primary damage production. Gao *et al.*<sup>27</sup> conducted similar simulations and reported that the PKA deposits most of its energy in the GBs. A bicrystal study on a selected GB [ $\Sigma 5$  twist (001)] in 3C-SiC has been carried out by Moriani *et al.*<sup>26</sup> Based on qualitative observations the authors reported that a significant fraction of radiation-induced defects is concentrated around the GB region.

Both Swaminathan *et al.*<sup>25</sup> and Gao *et al.*<sup>27</sup> reported quantitative analysis of defects in nc SiC, however these studies considered only random high angle GBs. It remains to be determined how defect production depends quantitatively on the GB type (including special low-angle GBs) in SiC and whether experimental observations of the decrease of radiation resistance in nc SiC can be attributed to the presence of low-energy GBs.<sup>33</sup> Special (often low-energy) GBs constitute ~12% of all GBs in 3C-SiC grown by chemical vapor deposition<sup>34</sup> and therefore these GBs could potentially have a measurable impact on radiation resistance of SiC.

## II. METHODS

### A. Interatomic potentials

MD simulations are carried out using the large-scale atomic/molecular massively parallel simulator (LAMMPS)<sup>35</sup> package. All simulations are performed on cubic (3C) SiC either in a single crystal (sc) or in a bicrystal configuration. Interatomic potentials for simulations of displacement cascades constitute an active area of research. In addition to the interactions at interatomic distances typical of a relaxed or a strained crystal, cascade simulations require a repulsive interaction at very close separations to better represent the ballistic and athermal processes that occur during ion bombardment. To model atomic interactions we use the hybrid Tersoff/ZBL potential.<sup>36–39</sup> More specifically, for all our studies in this work we use the SiC parameters of the Tersoff potential<sup>36–38</sup> as modified by Kohler.<sup>40</sup> This potential was used previously by Wojdyr<sup>41</sup> to generate GB structures in 3C-SiC. The parameters of this modified Tersoff potential capture formation of homonuclear bonds in GBs. It is to be noted that the parameters of the modified Tersoff potential used in the current study are different from the original Tersoff parameters<sup>36–38</sup> used previously by our group used for cascade simulations of nc-SiC (Ref. 25). In order to assess the effects of the potential parameters on defect production, we performed two sets of MD simulations (one with the original parameters and one with the modified Tersoff potential) and we compared defects produced in sc SiC between the two sets. We found that the total (cumulative) number of defects of all types produced while using the modified potential parameter set was between 5–15% in excess of the defects produced using the original parameter set.<sup>25</sup> However, statistics for individual defect types showed larger variations than those for the total number of defects. Specifically, carbon interstitials were between 3–13% in excess, while the carbon antisites were between 10–35% lower than what was produced with the original Tersoff potential. Production of carbon vacancies showed no change between the two potentials. The effects of the potential choice on the numbers of Si defects were stronger than the aforementioned effects on the number of C defects. Si vacancies, Si interstitials, and Si antisites, respectively, were 60–95%, 10–57%, and 21–42% higher when the modified potential was used. To avoid any artifacts associated with the choice of a potential, in this study we quantify the primary radiation damage using the total defect numbers (cumulative sum of all the individual defects), instead of considering any particular defect. We make this choice considering that the total defect counts agree between the two potential parameter sets within an acceptable error range, as mentioned above. In addition, we will always compare the damage between a cascade on a bicrystal to that of the sc using the same potential parameters.

### B. Bicrystal construction

SiC bicrystals were constructed based on the optimization scheme developed by Wojdyr *et al.*<sup>41</sup> All samples have a tilt axis of  $\langle 001 \rangle$  and consequently a (110) median plane.

It is instructive to discuss a few geometrical features of the SiC GBs. It was found<sup>41</sup> that GBs with the misorientation angle  $<13^\circ$  consist of dislocation cores separated by perfect crystalline regions [see Fig. 1(a)]. In contrast, in GBs with the misorientation angle  $>13^\circ$ , the dislocation cores overlap and individual dislocations can no longer be distinguished. These high angle GBs can be analyzed within the framework of the structural unit model<sup>42</sup> [Fig. 1(b)]. To explore a range of different structures, we have chosen for the analysis five low angle and four high angle, symmetric tilt GBs. The low angle GBs are:  $\Sigma 925$  ( $2.66^\circ$ ),  $\Sigma 365$  ( $4.24^\circ$ ),  $\Sigma 145$  ( $6.73^\circ$ ),  $\Sigma 85$  ( $8.80^\circ$ ), and  $\Sigma 61$  ( $10.40^\circ$ ). The high angle GBs chosen for our study are:  $\Sigma 13$  ( $22.62^\circ$ ),  $\Sigma 17$  ( $28.07^\circ$ ),  $\Sigma 5$  ( $36.87^\circ$ ), and  $\Sigma 37$  ( $71.00^\circ$ ). The number in the parentheses corresponds to the misorientation angle.

### C. Cascade simulations

Each bicrystal sample contains between  $\sim 2.03 \times 10^6$  and  $\sim 2.56 \times 10^6$  atoms. For the bicrystals, a Si PKA is chosen at a distance of  $17.24 \text{ \AA}$  (4 lattice constants) from the GB and it is given a velocity corresponding to 4 keV in a direction perpendicular to the GB (see Fig. 2). For low angle GBs [Fig. 1(a)] the PKA was chosen so that its velocity vector was directed toward the dislocation core, as opposed to a GB crystalline region between the dislocations. The sc sample consists of exactly  $1 \times 10^6$  atoms and it forms a cube with the edge length of  $216.44 \text{ \AA}$ . Periodic boundary conditions are applied in all three directions for both the sc and the bicrystal. A Langevin thermostat is applied to a  $8.66 \text{ \AA}$  thick layer of atoms on five sides of the sc and to all six sides of the bicrystal samples. The sixth side of the sc sample was close to the chosen Si PKA and no thermostat is maintained there to avoid introducing artificial energies to the cascade. This concern is not relevant for bicrystals, where the PKA atoms are chosen in the middle of the system. The thermostat temperature is set to 300 K.

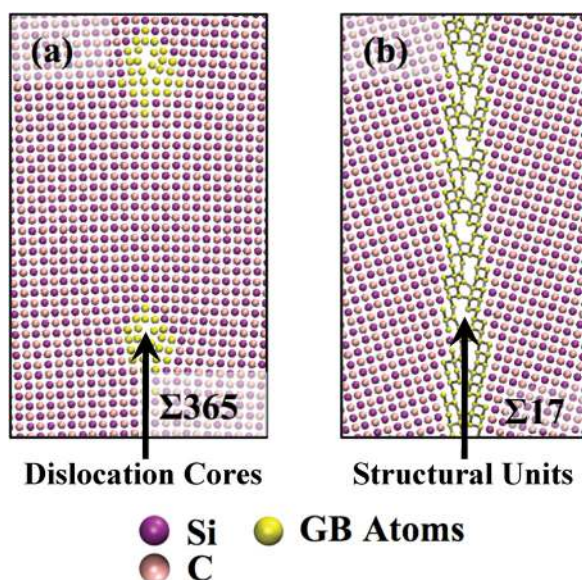


FIG. 1. (Color online) (a) A  $\Sigma 365$  ( $4.24^\circ$ ) GB consisting of dislocation cores separated by perfect crystalline regions. (b) A  $\Sigma 17$  ( $28.07^\circ$ ) GB, which consists of structural units.

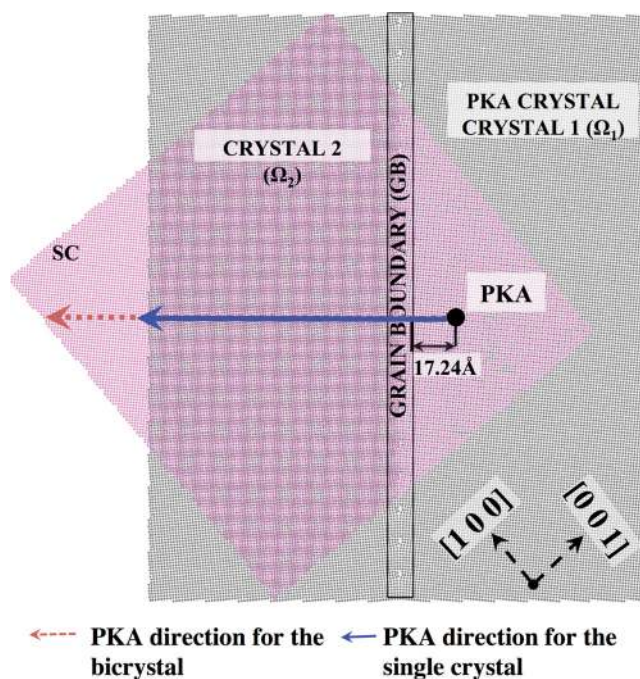


FIG. 2. (Color online) A schematic picture illustrating the idea of normalizing defect numbers in a bicrystal with respect to the PKA direction. In order to carry out such normalization, the PKA velocity direction in the sc is chosen to be identical to the PKA velocity direction in the grain containing the PKA atom ( $\Omega_1$ ).

The cascades were conducted in 5 phases (see Refs. 25 and 43 for details), which include thermal equilibration, thermostat-skin velocity scaling, initial cascade, intermediate evolution, and final equilibration.

### D. Defect analysis

Once cascade simulations have been completed, we analyze the atomic configurations to obtain information about defect distributions. Since we will analyze the nature of defect production in different subdomains of the bicrystal, we first identify the GB atoms and the in-grain atoms regions using common neighbor analysis (CNA).<sup>44</sup> Point defects are then identified using the Wigner-Seitz (or Voronoi cell analysis) since it is space filling and, unlike other commonly used methods, it is not based on a cut-off distance that is difficult to determine rigorously. Details of the methodology have been described in Ref. 25. Using this method we identify six types of defects that are possible in a binary system such as 3C-SiC: C vacancies ( $C_v$ ), Si vacancies ( $Si_v$ ), C antisites ( $C_{Si}$ ), Si antisites ( $Si_C$ ), C interstitials ( $C_i$ ), and Si interstitials ( $Si_i$ ). Defects in the GB are identified using the Voronoi boundary (VB) method.<sup>25</sup> According to this method, a defect is considered to be in the GB if it is in a Voronoi cell that belongs to the GB. As discussed in Ref. 25, the specific choice of a method for identifying GB defects does not affect the qualitative trends we observe in our radiation studies. When comparing defects produced in a bicrystal to those in a sc sample, the numbers are normalized by the volume of crystalline regions. The normalization is carried out using a mapping methodology developed in Ref. 25. Such a normalization is required to avoid spurious volume

exclusion effects, which occur for the following reason. In identifying the total number of in-grain defects in the bicrystal, we are excluding from the calculations the volume of GBs. Unless an equivalent volume is excluded from the corresponding sc data to which the bicrystal data is compared to, there will be a difference in the total defect numbers between the bicrystal and sc even if the density of defects is the same in the two cases. Moreover, the response of materials to external stimuli like radiation or external loading often depends on the density of the defects rather than their absolute numbers. For example, the ability of a material to resist radiation depends on the density of defects introduced per unit volume of the material and not on the total number of defects introduced. It is in this context that the defect normalization becomes important. The essence of the method is to compare defects in a sub-domain  $\Omega$  of the bicrystal to the defects in an equivalent region of the sc ( $sc_{eq}^\Omega$ ). Defect production is quantified by a fractional change in the number of defects  $p_\Omega$ , defined as

$$p_\Omega = \frac{D_\Omega - D_{sc_{eq}^\Omega}}{D_{sc_{eq}^\Omega}}, \quad (1)$$

where  $D_\Omega$  is the total number of defects in domain  $\Omega$  of the bicrystal and  $D_{sc_{eq}^\Omega}$  is the number of defects in the  $sc_{eq}^\Omega$ .

According to Eq. (1), when  $p_\Omega = 0$  the total numbers of defects produced in the bicrystal and sc samples are the same in domain  $\Omega$ . The lower limit  $p_\Omega$  is  $-1$  and it corresponds to no defects being produced in the domain  $\Omega$  of the bicrystal. The cases of  $p_\Omega > 0$ ,  $p_\Omega = 0$ , and  $p_\Omega < 0$  correspond to the GBs enhancing, not affecting, or suppressing the defect production in domain  $\Omega$ , respectively.

The values of  $D_{sc_{eq}^\Omega}$  in Eq. (1), which are used to normalize defect numbers in the bicrystals, were obtained by two different methods. In the first method, we determine  $D_{sc_{eq}^\Omega}$  by conducting cascades in the sc with its PKA velocity vector oriented along the  $[00\bar{1}]$  crystallographic direction. A total of 10 MD cascades (which we will call trials) were performed for the sc cascades. In this first method we then performed 90 trials (10 for each GB type) for the bicrystal samples with the PKA's velocity vector orientated perpendicular to the GBs. The second method directly takes into account the fact that the PKA's velocity in the bicrystal simulations deviates somewhat from the  $[00\bar{1}]$  direction, with the amount of deviation being dependent on the GB type. It is known that the threshold displacement energy surface of SiC is rather anisotropic.<sup>45,46</sup> The threshold displacement energy for Si atom was shown to vary from 35 to 101 eV while for C atom it varies from 30 to 62 eV. This can lead to the defect production rates being dependent on PKA direction. To isolate potential effects of the PKA direction on the defect production, we have carried out multiple cascades in sc with the PKA velocity oriented along the same crystallographic directions as those used in bicrystal simulations. Defects in the bicrystals were then normalized [using Eq. (1)] with respect to a sc with the same PKA velocity direction. Overall, to obtain adequate statistics, we conducted 20 trials (10 for bicrystal and 10 for sc) for each GB type totaling to 180 cascade simulations.

The various trials are made distinct by using different random seeds during the initial assignment of the velocities before the thermal equilibration phase (see Ref. 25). Such a scheme has been shown to be sufficient to achieve a complete decorrelation between the initial conditions and the configuration at end of the cascade development.<sup>47</sup> In assessing defect production rates ( $D_\Omega$  and  $D_{sc_{eq}^\Omega}$ ), the standard error of the mean is used as a measure of uncertainty in the data. The standard error of the mean is given by  $\sigma/\sqrt{n}$ , where  $\sigma$  is the standard deviation and  $n$  is the size of the sample. The errors in calculating  $D_\Omega$  ( $D_{sc_{eq}^\Omega}$ ) are appropriately propagated while calculating the error for  $p_\Omega$ .<sup>48</sup>

As mentioned above, we have limited ourselves to  $\approx 10$  trials per GB type to obtain meaningful statistics in a reasonable amount time. Furthermore, of the 10 trials, only those simulations which did not have defects in the thermostat region are considered for the analysis. Limiting to a small number of trials results in large error bars in the defect production and this is expected from MD simulations of cascades.<sup>47</sup> Obtaining more accurate averages of defect numbers would require a much larger number of cascade simulations (since the error bars decrease with the square root of the number of cascade simulations) or a use of a simplified approach like the binary collision approximation (BCA).<sup>47</sup> Therefore, to ensure that our claims are statistically significant, we perform an additional checks on the qualitative claims we make based on the values of  $p_\Omega$  for particular GB type. Specifically, for cases when  $p_\Omega > 0$  ( $p_\Omega < 0$ ), we test the null hypothesis  $H_0$ ,  $D_\Omega = D_{sc_{eq}^\Omega}$  against the alternative hypothesis  $H_1$ ,  $D_\Omega > D_{sc_{eq}^\Omega}$  or  $D_\Omega < D_{sc_{eq}^\Omega}$ , using Welch's modification of the student- $t$  test at a 0.05 significance level.<sup>49</sup> Thus, while we will use  $p_\Omega$  for guidance on defect production changes, we claim a particular defect production change is significant only when the alternative hypothesis  $H_1$  holds at a 0.05 significance level. For example, if we observed  $p_\Omega > 0$  we would claim a increase in defect production compared to the single crystal only if the associated alternative hypothesis  $D_\Omega > D_{sc_{eq}^\Omega}$  held at a 95% confidence level. We note that the null hypothesis implies  $p_\Omega = 0$  while the alternative hypothesis,  $D_\Omega > D_{sc_{eq}^\Omega}$  or  $D_\Omega < D_{sc_{eq}^\Omega}$  imply  $p_\Omega > 0$  or  $p_\Omega < 0$ , respectively.

### III. RESULTS AND DISCUSSION

#### A. Effect of GB on the defect production

##### 1. Defect production in the in-grain regions

We first discuss the fractional change in the total defect production in the in-grain (IG) regions of the bicrystal as compared to the sc. The in-grain defects are important because they are the ones that contribute to radiation-induced amorphization. Table I show the total in-grain defects in the bicrystal ( $D_{IG}$ ), the defects in equivalent regions of the sc ( $D_{sc_{eq}^{IG}}$  &  $D_{sc_{eq}^{IG}}$ ), and the corresponding values fractional change in the in-grain defect production ( $p_{IG}^\circ$  and  $p_{IG}$ ) for the two normalization approaches described in Sec. II D. The symbol “ $\circ$ ” indicates values that were obtained without normalizing the results with respect to the

TABLE I. Values of  $D_{IG}$ ,  $D_{sc_{eq}}^{\circ}$ ,  $p_{IG}^{\circ}$ ,  $D_{sc_{eq}}^{\circ}$  and  $p_{IG}$  for total the in-grain (IG) defects produced the bicrystal. The symbol, “ $\circ$ ” marks values that were obtained without normalizing the data with respect to the PKA direction.

GB	$D_{IG}$	$D_{sc_{eq}}^{\circ}$	$p_{IG}^{\circ}$	$D_{sc_{eq}}^{\circ}$	$p_{IG}$
$\Sigma 925$	$118 \pm 11$	$113 \pm 4$	$0.047 \pm 0.107$	$107 \pm 6$	$0.110 \pm 0.126$
$\Sigma 365$	$73 \pm 6$	$107 \pm 3$	$-0.323 \pm 0.060$	$80 \pm 7$	$-0.097 \pm 0.107$
$\Sigma 145$	$82 \pm 6$	$105 \pm 5$	$-0.221 \pm 0.069$	$82 \pm 6$	$-0.001 \pm 0.110$
$\Sigma 85$	$91 \pm 8$	$114 \pm 4$	$-0.200 \pm 0.075$	$105 \pm 8$	$-0.137 \pm 0.100$
$\Sigma 61$	$97 \pm 6$	$102 \pm 4$	$-0.048 \pm 0.067$	$84 \pm 9$	$0.155 \pm 0.143$
$\Sigma 13$	$89 \pm 7$	$102 \pm 4$	$-0.125 \pm 0.077$	$99 \pm 10$	$-0.102 \pm 0.111$
$\Sigma 17$	$124 \pm 5$	$119 \pm 4$	$0.036 \pm 0.050$	$113 \pm 8$	$0.089 \pm 0.082$
$\Sigma 5$	$87 \pm 7$	$119 \pm 4$	$-0.271 \pm 0.061$	$98 \pm 5$	$-0.111 \pm 0.082$
$\Sigma 37$	$100 \pm 4$	$118 \pm 3$	$-0.147 \pm 0.042$	$95 \pm 8$	$0.062 \pm 0.096$

PKA direction. The values of  $p_{IG}^{\circ}$  and  $p_{IG}$  for different GB types are also graphically shown in Figs. 3(a) and 3(b), respectively. Data in Fig. 3(a) shows negative values of  $p_{IG}^{\circ}$  for most GB types. The hypothesis tests performed also suggested the same qualitative behavior ( $D_{\Omega} < D_{sc_{eq}}^{\circ}$ ) for most of the GBs. This observation suggests that the presence of a GB suppresses the primary defect production. However, this data was obtained by normalizing bicrystal defects with respect to sc with the PKA aligned with the  $[00\bar{1}]$ , irrespectively of the GB type for which the defects are being calculated. In order to determine whether the defect suppression is the result of the PKA direction not being equivalent between the bicrystals and sc, we turn to Fig. 3(b), which shows defect numbers normalized for each bicrystal with respect to a sc with identical PKA direction. We find that for our number of trials the GB type does not have any statistically significant effect on the primary defect production in the crystalline regions. For all of the GB types the error bars are close to or cross zero and the production rates also test posi-

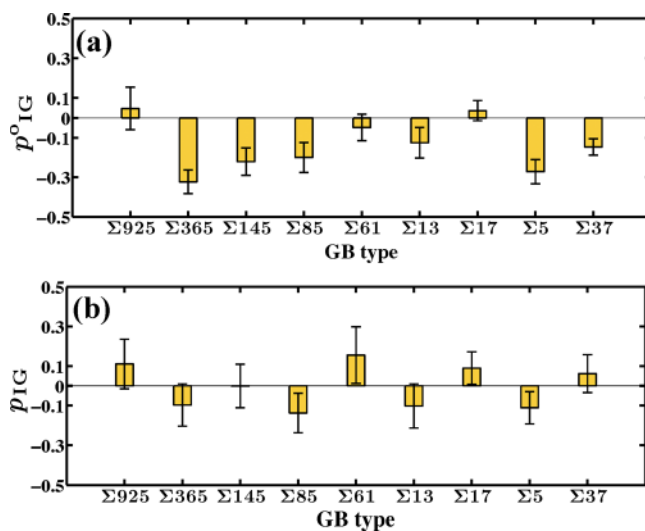


FIG. 3. (Color online) (a) The fractional change in defect production in the in-grain (IG) regions of the bicrystal in various GB types when the PKA direction for the sc is in the  $[00\bar{1}]$  direction. (b) The fractional change in defect production in the in-grain (IG) regions of the bicrystal in various GB types when the PKA direction for the sc is in the same crystallographic direction as the bicrystal.

tive for the null hypothesis, meaning there is no statistically significant change in defect production between the sc and bicrystal. This analysis demonstrates that the primary defect production depends on the PKA direction and it is important to take this effect into account when comparing results from bicrystals to those obtained for sc. In addition, when the results are normalized with respect to the PKA direction, it is found that GBs (irrespectively of their type) do not have any significant influence on the defect production.

## 2. Defect production in individual regions of the bicrystal

We now look at the defect production in the two in-grain regions of the bicrystal, namely CRYSTAL 1 ( $\Omega_1$ ) and CRYSTAL 2 ( $\Omega_2$ ) (see Fig. 2). It can be seen in Figs. 4(a) and 4(b) that the fractional change in defect production in either  $\Omega_1$  [Fig. 4(a)] or  $\Omega_2$  [Fig. 4(b)], is zero for many of the GB types studied (See Table II and Table III for values).  $\Sigma 13$  however, shows a positive defect production in  $\Omega_1$  and negative in  $\Omega_2$ .  $\Sigma 85$  shows a negative defect production in  $\Omega_2$  while no change with respect to the sc in  $\Omega_1$  while  $\Sigma 365$  shows the opposite trend. As was shown in Fig. 3(b), defect production in the total in-grain regions (which includes both  $\Omega_1$  and  $\Omega_2$ ) is unaffected by the presence of the GB. On testing the appropriate hypothesis for each of these GB types and in both domains, we had to accept the null hypothesis ( $D_{\Omega} = D_{sc_{eq}}^{\circ}$ ) for all but  $\Sigma 13$  in the domain  $\Omega_1$ . While this one result is significant at the 95% confidence level, we do not think it actually shows a change in defect production associated with this grain boundary. We have assessed enough cases in this work that obtaining at least one false result with 95% confidence is actually quite likely. Furthermore, the asymmetry in defect production observed for  $\Sigma 13$  from the values of  $p_{\Omega}$  is not mirrored in the hypothesis tests, which only show significance for the  $\Omega_1$  domain. Given that the total defect production in the in-grain region for  $\Sigma 13$  was zero [see Fig. 3(b)] a positive value in  $\Omega_1$  must imply a negative defect production in  $\Omega_2$ , which is not observed on

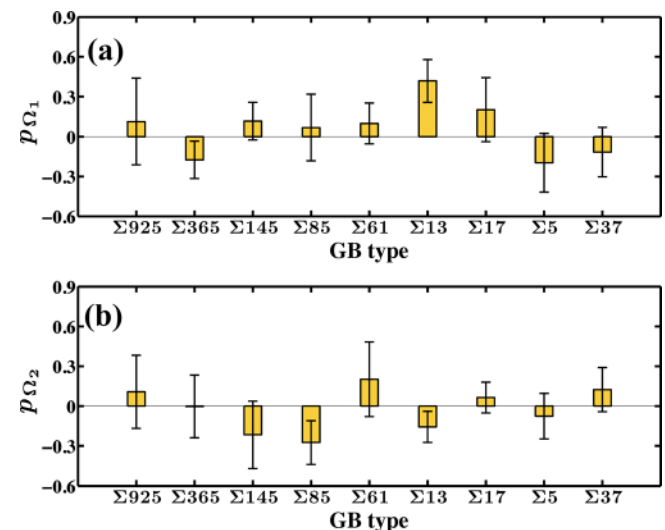


FIG. 4. (Color online) The fractional change in defect production in (a) CRYSTAL 1 ( $\Omega_1$ ) and (b) CRYSTAL 2 ( $\Omega_2$ ).

TABLE II. Values of  $D_{\Omega_1}$ ,  $D_{sc\Omega_1}$ , and  $p_{\Omega_1}$  for the defects produced in CRYSTAL 1 ( $\Omega_1$ ).

GB	$D_{\Omega_1}$	$D_{sc\Omega_1}$	$p_{\Omega_1}$
$\Sigma 925$	$51 \pm 13$	$45 \pm 6$	$0.114 \pm 0.325$
$\Sigma 365$	$36 \pm 3$	$44 \pm 6$	$-0.175 \pm 0.141$
$\Sigma 145$	$59 \pm 5$	$53 \pm 5$	$0.117 \pm 0.142$
$\Sigma 85$	$45 \pm 10$	$42 \pm 4$	$0.068 \pm 0.250$
$\Sigma 61$	$42 \pm 3$	$38 \pm 4$	$0.100 \pm 0.154$
$\Sigma 13$	$13 \pm 1$	$9 \pm 1$	$0.419 \pm 0.160$
$\Sigma 17$	$25 \pm 5$	$21 \pm 2$	$0.203 \pm 0.240$
$\Sigma 5$	$23 \pm 3$	$28 \pm 7$	$-0.196 \pm 0.221$
$\Sigma 37$	$22 \pm 4$	$25 \pm 3$	$-0.116 \pm 0.186$

performing the hypothesis test. Finally, we note that there is no physical reason apparent to us that  $\Sigma 13$  should be the only GB type to produce a change in defect production rates. Therefore, we feel that this anomalous behavior of  $\Sigma 13$  arose out of our limited statistics and there is no evidence from the production rates for this GB actually affecting the morphology of the cascade.

It is instructive to compare the effect of GBs on the in-grain damage we observed in SiC to other nonmetals on which bicrystal cascade simulations have been conducted, to the extent such comparison is possible. Of particular interest is the study by Brutzel *et al.*<sup>28</sup> who investigated  $UO_2$  bicrystals and reported a non-negligible effect of the GBs on the in-grain defect production. Because in the  $UO_2$  study defect numbers in bicrystals have not been normalized to a sc cascade with an equivalent volume and/or with equivalent PKA direction (see Sec. II D), a quantitative comparison to our study is not possible. At this point, it is unclear whether normalization with PKA direction is necessary for  $UO_2$ , since different interatomic potentials seem to lead to different conclusions on the issue of defect production versus PKA direction.<sup>28,50</sup> However, there are a number of qualitative variations between the two materials that could possibly explain the reported differences in their response to radiation.  $UO_2$  and SiC have different masses, crystallographic structures and ionicity of bonding, which may affect both the GB structure and how the radiation cascade develops in these materials. In fact, cascade morphology in  $UO_2$  is quite distinct from the cascade morphology in SiC. In the study of

TABLE III. Values of  $D_{\Omega_2}$ ,  $D_{sc\Omega_2}$ , and  $p_{\Omega_2}$  for the defects produced in CRYSTAL 2 ( $\Omega_2$ ).

GB	$D_{\Omega_2}$	$D_{sc\Omega_2}$	$p_{\Omega_2}$
$\Sigma 925$	$68 \pm 13$	$61 \pm 9$	$0.107 \pm 0.275$
$\Sigma 365$	$36 \pm 6$	$36 \pm 6$	$-0.003 \pm 0.236$
$\Sigma 145$	$23 \pm 6$	$29 \pm 5$	$-0.216 \pm 0.252$
$\Sigma 85$	$46 \pm 8$	$63 \pm 9$	$-0.274 \pm 0.164$
$\Sigma 61$	$55 \pm 6$	$46 \pm 9$	$0.202 \pm 0.281$
$\Sigma 13$	$76 \pm 7$	$90 \pm 9$	$-0.157 \pm 0.117$
$\Sigma 17$	$99 \pm 7$	$93 \pm 8$	$0.064 \pm 0.116$
$\Sigma 5$	$64 \pm 9$	$70 \pm 9$	$-0.076 \pm 0.172$
$\Sigma 37$	$79 \pm 6$	$70 \pm 9$	$0.124 \pm 0.166$

Brutzel *et al.*<sup>28</sup>  $UO_2$  cascades have a spherical shape, which is centered at the GB and therefore the GB constituted a significant part of the cascade volume. In contrast, cascades in SiC (both sc and bicrystal) have a rather elongated morphology as shown in Fig. 5. Similar morphologies for sc SiC have been reported by Devanathan *et al.*<sup>51</sup> in simulations with a larger PKA energy (10 keV) than the one considered in our study (4 keV). Another difference between SiC and  $UO_2$  is that defects in  $UO_2$  seem to be more mobile. In contrast to the  $UO_2$  study, no defect diffusion was observed in our irradiated studies of SiC on MD time scales. In summary, more quantitative analysis needs to be carried out to identify how much the effects of GBs on in-grain defect production depend on a specific material and what is the physics that underlies these differences.

## B. Effect of cascade on the GB

Having discussed the effects of GBs on the radiation cascade, we now turn to the question of the effect of displacement cascades on the GB structures. The total number of GB defects ( $D_{GB}$ ), the total number of defects in an equivalent sc ( $D_{sc\Omega_1}$ ), and the fractional change in defects ( $p_{GB}$ ) are reported in Table IV. The values of  $p_{GB}$  are also represented graphically in Fig. 6. It can be seen that some of the GBs, such as  $\Sigma 85$ ,  $\Sigma 145$ , and  $\Sigma 5$ , show a positive value of  $p_{GB}$ , indicating an enhanced defect production as compared to sc. However, only for  $\Sigma 85$  and  $\Sigma 5$  did the hypothesis test also confirm the same qualitative behavior. Other GB types had their error bars crossing zero and also agreed with the null hypothesis, thereby showing no change of defect production from the sc. An enhanced defect production in SiC GBs has been previously reported from studies on nc samples, which samples consisted of a network of high-energy random GBs.<sup>25</sup> It was postulated that amorphous-like high-energy GB have a lower threshold displacement energy than sc samples, although these threshold displacement energies have not been yet measured directly.

One reason some GBs show positive relative changes in defect production while others show little change could be the effect of local stresses on the threshold displacement energy of atoms constituting the GB. It is well known that GBs consist of alternating compressive and tensile regions<sup>52</sup> and it has been recently shown for SWNT and for Si nanowire<sup>53</sup> that the threshold displacement energy can be a function of strain. We hypothesize that if the cascade sampled primarily a specific region of the GB, it could lead to slight

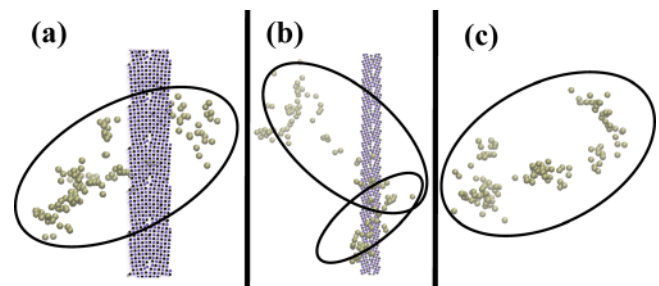
FIG. 5. (Color online) Typical defect distribution morphology of (a)  $\Sigma 61$ , (b)  $\Sigma 5$ , and (c) single crystal.

TABLE IV. Values of  $D_{GB}$ ,  $D_{sc^{GB}}$ , and  $p_{GB}$  for the defects produced in the grain boundary (GB).  $D_{sc^{GB}}$  is the number of defects in an equivalent region of the sc which is at the same distance from the PKA as in the corresponding bicrystal.

GB	$D_{GB}$	$D_{sc^{GB}}$	$p_{GB}$
$\Sigma 925$	$28 \pm 8$	$30 \pm 7$	$-0.072 \pm 0.336$
$\Sigma 365$	$56 \pm 8$	$51 \pm 6$	$0.082 \pm 0.205$
$\Sigma 145$	$66 \pm 8$	$53 \pm 6$	$0.256 \pm 0.205$
$\Sigma 85$	$52 \pm 9$	$34 \pm 6$	$0.540 \pm 0.366$
$\Sigma 61$	$48 \pm 7$	$57 \pm 11$	$-0.159 \pm 0.213$
$\Sigma 13$	$53 \pm 11$	$35 \pm 9$	$0.535 \pm 0.520$
$\Sigma 17$	$19 \pm 5$	$16 \pm 6$	$0.137 \pm 0.552$
$\Sigma 5$	$64 \pm 10$	$44 \pm 6$	$0.474 \pm 0.299$
$\Sigma 37$	$41 \pm 4$	$39 \pm 7$	$0.041 \pm 0.216$

differences in the measured defect productions among different GB types.

Now that we have seen that the cascade can produce damage in the GB, it is interesting to ask how radiation affects the chemical order in SiC. 3C-SiC has a zinc-blende structure with every Si atom bonded to four other C atom and vice versa. Therefore, a perfect structure of sc SiC is entirely composed of heteronuclear bonds. Creation of antisite defects is accompanied by formation of homonuclear bonds. Antisite accumulation has been postulated to be an important process leading to radiation-induced amorphization of SiC.<sup>54</sup> In an amorphous SiC, the ratio ( $\chi$ ) of the number of homonuclear bonds to heteronuclear bonds has been reported to range between 0.13 and 0.5.<sup>55</sup> We note that GBs in our bicrystal samples are already comprised of some atoms with homonuclear bonds as was mentioned in Sec. II A. To determine the change in chemical disorder due to irradiation, we calculate the values of  $\chi$  before and after cascade simulations. In addition, because the cascade was found to interact only with a small region of the GB (see Fig. 5), to obtain reasonable statistics we adopt the following scheme in our calculations. First, we calculate  $\chi$  only in the regions of the GB which was irradiated (damaged by the cascade). This value is then compared to the value of  $\chi$  calculated in the same region of the nonirradiated structure. Figure 7(a) shows  $\chi$  for the both the nonirradiated and irradiated GBs. To demonstrate that the cascade has settled and the defect numbers do not change within the time scales of MD simulations, in Fig. 7(a) we report values of  $\chi$  calculated after 5.5 and 6.5 ps.

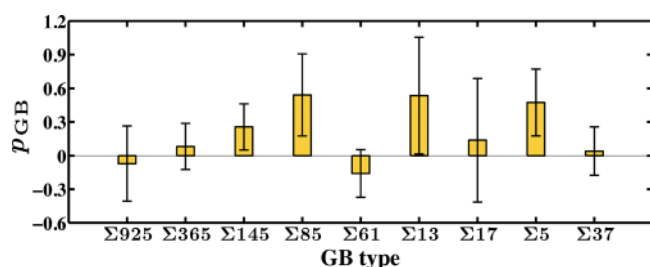


FIG. 6. (Color online) Defect production in the GB.

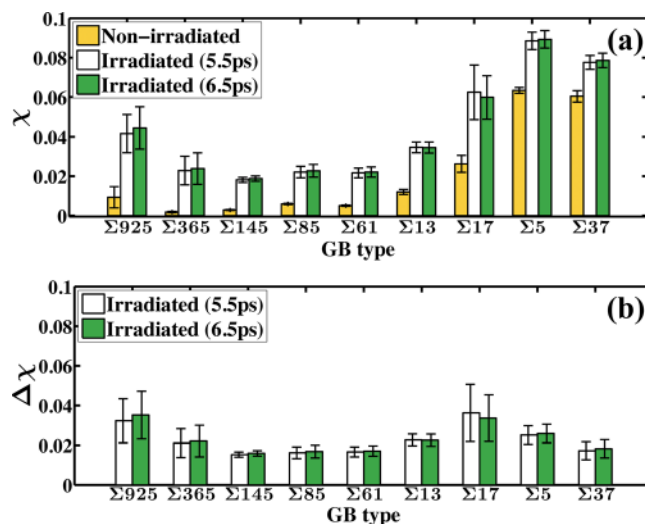


FIG. 7. (Color online) (a) The ratio of homonuclear to heteronuclear bonds ( $\chi$ ) in the irradiated GB region compared to  $\chi$  in equivalent regions of the nonirradiated GB. The numbers within parentheses indicate the time for which the system were relaxed following the cascade. (b) The difference between the values of  $\chi$  in irradiated and nonirradiated GBs ( $\Delta\chi$ ).

We find that prior to irradiation,  $\chi$  increases almost monotonically with the misorientation angle. This observation can be explained by the fact that the low angle GBs are comprised of regions of perfect (although strained) crystalline lattice separated by occasional dislocation cores, as shown in Fig. 1(a). The nonzero value of  $\chi$  arises primarily from atoms in the dislocation cores. As the misorientation angle is increased, the dislocation cores become more closely spaced and  $\chi$  increases. At misorientation angles  $>13^\circ$  the dislocation cores merge and no perfect crystalline regions are present within the GB [see Fig. 1(b)]. Consequently, the value of  $\chi$  is also seen to be higher. The white and the dark gray (green online) bars in Fig. 7, which show values of  $\chi$  for irradiated GBs, follow a similar trend with the misorientation angle as observed for the nonirradiated GBs. Additionally,  $\chi$  increases due to irradiation in all the GBs under study.

In order to determine whether GB type has any effect on the radiation-induced chemical disorder, in Fig. 7(b) we plot the difference  $\Delta\chi$  between  $\chi$  calculated for irradiated and nonirradiated samples. Since  $\Delta\chi$  is comparable among the different GBs, we conclude that the effect of radiation on chemical disorder does not depend on the GB misorientation angle or GB energy.

#### IV. CONCLUSION

We determined how primary radiation damage depends on the type of GB in 3C-SiC and how the GB structures are altered by radiation. Five low angle and four high angle GBs were chosen for the study. We demonstrated that in SiC the direction of the PKA velocity has a significant effect on defect production. Without normalizing the damage with respect to the PKA direction, GBs appear to suppress the primary damage production as compared to a single crystal SiC. However, after correctly normalizing with respect to the PKA direction, we find that in-grain defect production is not

affected by the presence of a GB, independently of its type. The defect production in the individual domains comprising the in-grains regions were also examined. The results seem to indicate that none of the GB types affect the cascade morphology in such a way as to alter the defect production compared to sc in the two sides of the bicrystal.

The damage and defect production in the GB regions were also examined. A few GB types showed a positive fractional change of the defects while others show no difference when compared to equivalent regions of the sc. The observed differences between GB types may be related to the stress distribution that is specific to each GB and to the fact that an isolated cascade interacts with a relatively small region within the GB. We analyzed the radiation-induced chemical disorder in the GBs and quantified it by the homonuclear to heteronuclear bond ratio ( $\chi$ ). We found that  $\chi$  increases nearly monotonically with the misorientation angle, which behavior has been attributed to the decreasing distance between dislocation cores with an increasing misorientation angle. We found that the change in the chemical disorder due to irradiation does not depend on the type of the GB.

The total damage in the in-grain regions was found to be unaffected by the GB types and so is the damage in the individual domains constituting the in-grain regions. We conclude that further studies are needed to determine threshold displacement energies in GBs and how they compare to the corresponding values in the bulk crystalline material.

## ACKNOWLEDGMENTS

This work was supported by the U.S. Department of Energy, Office of Basic Energy Sciences under grant number DE-FG02-08ER46493. Computational time was provided in part by the National Science Foundation through TeraGrid resources provided by Texas Advanced Computing Center (Ranger systems) under grant number TG-DMR090097.

- <sup>1</sup>I. Szlufarska, A. Nakano, and P. Vashishta, *Science* **309**, 911 (2005).
- <sup>2</sup>I. Szlufarska, *Mater. Today* **9**, 42 (2000).
- <sup>3</sup>H. Gleiter, *Acta Mater.* **48**, 1 (2000).
- <sup>4</sup>F. Liao, S. L. Girshick, W. M. Mook, W. W. Gerberich, and M. R. Zachariah, *Appl. Phys. Lett.* **86**, 171913 (2005).
- <sup>5</sup>R. W. Siegel, *Nanomaterials: Synthesis, Properties and Applications* (IOP, 1996), Chap. "Nanostructures of Metals and Ceramics", p. 201, Bristol 1996 ed.
- <sup>6</sup>X. T. Wang, N. P. Padture, H. Tanaka, and A. L. Ortiz, *Acta Mater.* **53**, 271 (2005).
- <sup>7</sup>Committee, U. D. N. E. R. A., and the Generation IV International Forum. A technology roadmap for the generation iv nuclear energy systems. Tech. Rep. GIF00200, INEEL, 2002.
- <sup>8</sup>T. R. Allen and D. C. Crawford, Proceedings of ICAPP '03, Cordoba, Spain, American Nuclear Society, 3237 (2003).
- <sup>9</sup>M. Ishimaru, I.-T. Bae, A. Hirata, Y. Hirotsu, J. A. Valdez, and K. E. Sickafus, *Phys. Rev. B* **72**, 024116 (2005).
- <sup>10</sup>V. I. Ivashchenko, P. E. A. Turchi, and V. I. Shevchenko, *Phys. Rev. B* **75**, 085209 (2007).
- <sup>11</sup>M. Rose, A. G. Balogh, and H. Hahn, *Nucl. Instrum. Methods Phys. Res. B* **127/128**, 119 (1997).
- <sup>12</sup>J. Zhang, J. Lian, S. Fuentes, Antonio, F. Zhang, M. Lang, F. Lu, and C. Ewing, Rodney, *Appl. Phys. Lett.* **94**, 243110 (2009).
- <sup>13</sup>T. D. Shen, *Nucl. Instrum. Methods B* **266**, 921 (2008).
- <sup>14</sup>H. Wang, R. Araujo, J. G. Swadener, Y. Q. Wang, X. Zhang, E. G. Fu, and T. Cagin, *Nucl. Instrum. Methods Phys. Res. B* **261**, 1162 (2007).
- <sup>15</sup>Y. Chimi, A. Iwase, N. Ishikawa, M. Kobiyama, T. Inami, and S. Okuda, *J. Nucl. Mater.* **297**, 355 (2001).
- <sup>16</sup>A. Meldrum, A. Boatner, and C. Ewing, *R. Phys. Rev. Lett.* **88**, 25503 (2003).
- <sup>17</sup>B. Johannessen, P. Kluth, D. Llewellyn, G. J. Foran, D. J. Cookson, and M. C. Ridgway, *Appl. Phys. Lett.* **90**, 073119 (2007).
- <sup>18</sup>M. Samaras, P. M. Derlet, H. Van Swygenhoven, and M. Victoria, *Phys. Rev. Lett.* **88**, 125505 (2002).
- <sup>19</sup>M. Samaras, P. M. Derlet, H. Van Swygenhoven, and M. Victoria, *Philos. Mag.* **83**, 3599 (2003), sp. Iss. SI.
- <sup>20</sup>M. Samaras, P. M. Derlet, H. Van Swygenhoven, and M. Victoria, *J. Nucl. Mater.* **351**, 47 (2006).
- <sup>21</sup>R. E. Stoller, P. J. Kamenski, and Y. N. Osetsky, in *Mater. Res. Soc. Symp. Proc.* **1125**, r05 (2009).
- <sup>22</sup>P. C. Millett, D. S. Aidhy, T. Desai, S. R. Phillipot, and D. Wolf, *Int. J. Mater. Res.* **100**, 550 (2009).
- <sup>23</sup>P. C. Millett, D. Wolf, T. Desai, and V. Yamakov, *Appl. Phys. Lett.* **93**, 161902 (2008).
- <sup>24</sup>X.-M. Bai, A. F. Voter, R. G. Hoagland, M. Nastasi, and B. P. Uberuaga, *Science* **327**, 1631 (2010).
- <sup>25</sup>N. Swaminathan, P. J. Kamenski, D. Morgan, and I. Szlufarska, *Acta Mater.* **58**, 2843 (2010).
- <sup>26</sup>A. Moriani and F. Cleri, *Phys. Rev. B* **73**, 214113 (2006).
- <sup>27</sup>F. Gao, D. Chen, W. Hu, and W. J. Weber, *Phys. Rev. B* **81**, 184101 (2010).
- <sup>28</sup>L. Van Brutzel and E. Vincent-Aublant, *J. Nucl. Mater.* **377**, 522 (2008).
- <sup>29</sup>L. Van Brutzel, E. Vincent-Aublant, and J. M. Delaye, *Nucl. Instrum. Methods B* **267**, 3013 (2009).
- <sup>30</sup>E. Vincent-Aublant, J. M. Delaye, and L. Van Brutzel, *J. Nucl. Mater.* **392**, 114 (2009).
- <sup>31</sup>X.-M. Bai and B. P. Uberuaga, *Philos. Mag.* **1** (2012), doi:10.1080/14786435.2011.648229.
- <sup>32</sup>W. Jiang, H. Wang, I. Kim, I.-T. Bae, I. G. Li, P. Nachimuthu, Z. Zhu, Y. Zhang, and J. Weber, *Phys. Rev. B* **80**, 161301 (2009).
- <sup>33</sup>W. Jiang, H. Wang, I. Kim, Y. Zhang, and W. J. Weber, *J. Mater. Res.* **25**, 12 (2010).
- <sup>34</sup>L. Tan, T. Allen, J. Hunn, and J. Miller, *J. Nucl. Mater.* **372**, 400 (2008).
- <sup>35</sup>S. J. Plimpton, *J. Comput. Phys.* **117**, 1 (1995).
- <sup>36</sup>J. Tersoff, *Phys. Rev. B* **39**, 5566 (1989).
- <sup>37</sup>J. Tersoff, *Phys. Rev. Lett.* **64**, 1757 (1990).
- <sup>38</sup>J. Tersoff, *Phys. Rev. B* **49**, 16349 (1994).
- <sup>39</sup>J. F. Ziegler, J. P. Biersack, and U. Littmark, *The Stopping Range of Ions in Solids* (Pergamon, New York, 1985).
- <sup>40</sup>C. Kohler, *Phys. Status Solidi B* **234**, 522 (2002).
- <sup>41</sup>M. Wojdyr, S. Khalil, Y. Liu, and I. Szlufarska, *Model. Simul. Mater. Sci.* **18**, 075009 (2010).
- <sup>42</sup>A. P. Sutton and V. Vitek, *Philos. Trans. R. Soc. London, Ser. A* **309**, 1 (1983).
- <sup>43</sup>D. E. Farrell, N. Bernstein, and W. K. Liu, *J. Nucl. Mater.* **385**, 572 (2009).
- <sup>44</sup>J. D. Honeycutt and H. C. Andersen, *J. Phys. Chem.* **91**, 4950 (1987).
- <sup>45</sup>L. Malerba and J. M. Peraldo, *Phys. Rev. B* **65**, 045202 (2002).
- <sup>46</sup>J. M. Peraldo, L. Malerba, A. Sanchez-Rubio, and T. Diaz de la Rubia, *J. Nucl. Mater.* **276**, 235 (2000).
- <sup>47</sup>M. Hou, A. Souidi, and C. S. Becquart, *J. Phys.: Condens. Matter* **13**, 5365 (2001).
- <sup>48</sup>J. R. Taylor, *An Introduction to Error Analysis*, 2nd ed. (University Science Books, Sausalito, CA, 1997).
- <sup>49</sup>R. V. Hogg and E. A. Tanis, *Probability and Statistical Inference*, 5th ed. (Prentice-Hall, New Jersey, 1997).
- <sup>50</sup>C. Meis and A. Chartier, *J. Nucl. Mater.* **341**, 25 (2005).
- <sup>51</sup>R. Devanathan, *Nucl. Instrum. Meth. B* **141**, 118 (1998).
- <sup>52</sup>J. P. Hirth and J. Lothe, *Theory of dislocation* (McGraw-Hill, New York, 1968).
- <sup>53</sup>E. Holmström, L. Toikka, A. V. Krashenninnik, and K. Nordlund, *Phys. Rev. B* **82**, 045420 (2010).
- <sup>54</sup>X. L. Yuan and L. W. Hobbs, *Nucl. Instrum. Methods Phys. Res. B* **191**, 74 (2002).
- <sup>55</sup>R. Devanathan, F. Gao, and W. Weber, *Nucl. Instrum. Methods Phys. Res. B* **255**, 130 (2007).